Journal of Hazardous Materials 227–228 (2012) 211–218

Contents lists available at SciVerse ScienceDirect

Journal of Hazardous Materials

journal homepage: www.elsevier.com/locate/jhazmat

Mechanism insights into enhanced Cr(VI) removal using nanoscale zerovalent iron supported on the pillared bentonite by macroscopic and spectroscopic studies

Yimin Li*, Jianfa Li, Yuling Zhang

College of Chemistry and Chemical Engineering, Shaoxing University, Zhejiang 312000, PR China

HIGHLIGHTS

- Al-bent enriched Cr(VI) on NZVI surface, leading to the enhanced removal.
- The NZVI/Al-bent composite exhibited good stability and reusability.
- XAFS results showed transfer of precipitates from iron surface to Al-bent.

ARTICLE INFO

Article history:
Received 8 February 2012
Received in revised form 7 May 2012
Accepted 9 May 2012
Available online 15 May 2012

Keywords:
Pillared bentonite
Nanoscale zerovalent iron
Removal
Hexavalent chromium
X-ray absorption fine structure (XAFS)

ABSTRACT

NZVI was supported on a pillared bentonite (Al-bent) to enhance the reactivity of NZVI and prevent its aggregation. The performance and mechanisms of the combined NZVI/Al-bent on removing hexavalent chromium (Cr(VI)) was investigated by batch and XAFS experiments. The batch investigations indicated that Cr(VI) could be almost completely removed by NZVI/Al-bent after 120 min. The efficiency was not only much higher than that by NZVI (63.0%), but also superior to the sum of NZVI reduction and Al-bent adsorption (12.4%). Besides, NZVI/Al-bent exhibited good stability and reusability, and Al-bent could reduce the amount of iron ions released into the solution. XANES results provided evidence that NZVI/Al-bent could reduce Cr(VI) entirely into Cr(III), while NZVI reduced Cr(VI) partly into Cr(III) with a trace of Cr(VI) adsorbed on the corrosion products. The structure of Cr(VI)-treated NZVI/Al-bent determined with EXAFS revealed the formation of Cr–Al/Si bond, suggesting that some insoluble Cr(III) species might be transferred to the surface of Al-bent, therefore the precipitates on iron surface could be greatly reduced. The results demonstrated that Al-bent plays a significant role in enhanced reactivity and stability of NZVI, and may shed new light on design and fabrication of supported NZVI for environmental remediation.

1. Introduction

Zerovalent iron (ZVI) has been extensively investigated over the past decades as an environmentally benign chemical reductant for remediation of a variety of contaminants including chlorinated organics [1,2], nitroaromatics [3], radionuclides [4,5] and heavy metals [6–8]. Because the reduction of contaminants occurs on the solid iron surface, the smaller size of ZVI particles means larger specific surface area, and consequently results in higher reactivity. Therefore, nanoscale zerovalent iron (NZVI) has received more attention on removing contaminants in recent years [9–11]. However, there are still some technical challenges associated with NZVI application, for example, how to prevent its aggregation and to enhance its stability and reusability [12–14]. In order to solve these problems, NZVI immobilization on mechanical supports such as resins [9,10], porous carbon [15–17] and polymers like CMC [18,19] and PVP [19] has been attempted. For example, Ponder et al. [9,10] have demonstrated that the removal rates of Cr(VI) and Pb(II) by resin supported NZVI were enhanced by 5 and 18-fold, respectively, in comparison with that by bare NZVI. NZVI has also been incorporated into silica particles by Zheng et al. [20] using an aerosol-assisted process and subsequent reduction, and more efficient TCE treatment without NZVI aggregation was obtained. All of these results suggest that supported NZVI is a promising candidate for remediation of contaminated sites [15–17,20,21]. However, some of these immobilization methods are complex, and development of more efficient immobilization system is always desirable for promoting the practical applications of NZVI.

Bentonite, as a low cost adsorbent, is a kind of natural clay consisting mainly of layered montmorillonite, and has been under

* Corresponding author at: College of Chemistry and Chemical Engineering, Shaoxing University, Huancheng West Road 508, Shaoxing, Zhejiang 312000, China. Tel.: +86 575 8834 2386; fax: +86 575 8831 9253.
E-mail address: liym@usx.edu.cn (Y. Li).

0304-3894/$ – see front matter © 2012 Elsevier B.V. All rights reserved.
http://dx.doi.org/10.1016/j.jhazmat.2012.05.034

extensive investigations for remediation of contaminants due to its abundance, chemical stability and high adsorption capability [22]. Recently, bentonite has been used as a support for NZVI immobilization [23], and Cr(VI) removal was enhanced by using bentonite supported NZVI instead of bare NZVI. In comparison with above-mentioned supports, bentonite is superior because it can be easily modified by intercalating inorganic or organic cations into the montmorillonite interlayers [24,25]. So it is feasible to introduce different functional groups into bentonite according to the structure and property of target contaminants, and fabricate pillared bentonites with enhanced adsorption to the particular contaminants. According to our previous research on the NZVI supported on pillared bentonites, the enhanced adsorption by bentonites has resulted in the surprising advance on NZVI reactivity. For example, NZVI supported on poly(hydroxo Al(III)) cations-pillared bentonite (Al-bent) resulted in the enhanced nitrate removal [26], while NZVI supported on hydrophobic organobentonite showed enhanced removal of organic contaminants [27,28]. Despite the compelling results on the enhanced removal of various contaminants by using NZVI supported on pillared bentonites, the understanding on mechanisms responsible for the enhancement is still insufficient due to the complexity of this novel supported NZVI system.

Herein, a spectroscopic technique namely X-ray absorption fine structure (XAFS) is employed to probe the mechanisms for the enhanced Cr(VI) removal by Al-bent supported NZVI as observed in batch experiments. The postulates of this work are as following: (1) immobilization of NZVI on Al-bent may make NZVI less prone to aggregation, while enhancing its reactivity; (2) the pillared bentonite (Al-bent) as an enhanced adsorbent for Cr(VI) will have the contaminant concentrated at reaction sites and thus promote the driving force of reaction; (3) some insoluble Cr(III) species produced during reaction may be transferred to Al-bent surface, hence, the reusability of the NZVI/Al-bent system is obviously increased.

2. Materials and methods

2.1. Materials and chemicals

The original bentonite (Na-bent) mainly composed of Na^+–montmorillonite was purchased from Inner Mongolia (China), with its cation exchange capacity of 115 cmol/kg determined by ammonium acetate method [29]. Commercial iron and other chemicals of analytical grade were all purchased from Shanghai Chemical Co., China. The fraction of iron powder passing through a sieve of 0.15 mm was used. The detailed methods for preparation and characterizations of Al-bent, NZVI and NZVI/Al-bent have been described in our previous work [26]. The BET specific surface areas were determined to be 0.350 m^2/g for commercial iron powder (ZVI), 33.5 m^2/g for NZVI, 29.8 m^2/g for NZVI/Al-bent and 47.4 m^2/g for NZVI/Na-bent, respectively. The iron contents of NZVI, NZVI/Al-bent and NZVI/Na-bent samples were measured to be 53.6%, 23.9% and 18.9%, respectively.

The stock Cr(VI) solution was prepared by dissolving potassium dichromate in de-ionized water. The solution pH was adjusted by adding 0.1 mol/L HCl or 0.1 mol/L NaOH solution, and measured together with pH changes during the reaction with a pH meter (PHS-3C, China).

2.2. Adsorption isotherm

Adsorption isotherms of Cr(VI) on Na-bent and Al-bent were determined by using batch equilibrium of 0.1 g Na-bent or Al-bent in 25 mL Cr(VI) solution at various initial concentrations. The adsorption experiments were carried out in a thermostatic shaker bath at 25 ± 0.1 °C for 120 min. After equilibrium, the suspension was centrifuged and filtered through a 0.22 μm membrane, and Cr(VI) concentration in supernatant was measured by the diphenyl carbazide method on a UV–vis spectrophotometer (722, Shanghai Spectrum) at 540 nm [30]. The adsorbed amount (Q_e) was calculated from the difference between initial (C_0 (mg/L)) and equilibrium (C_e (mg/L)) concentration according to the equation, $Q_e = [(C_0 - C_e) \times V]/m$, where V is the total volume of solution (mL), and m is the mass of adsorbent (g).

2.3. Batch experiments for Cr(VI) removal

The removal of Cr(VI) was conducted in conical flask containing 100 mL of Cr(VI) solution (initial pH 5.6, and initial concentration C_0 = 50 mg/L, unless otherwise specified). Four zerovalent iron sources including commercial iron (0.050 g), NZVI (0.0932 g), NZVI/Na-bent (0.265 g) and NZVI/Al-bent (0.209 g) were added in the Cr(VI) solution, respectively. In these treatments, the four iron sources were used at the same dosage of iron of 0.500 g/L. Al-bent alone was also used in a separate treatment, and the dosage (0.159 g) was same as that used in the NZVI/Al-bent. The Cr(VI) solution was deoxygenated by N_2 stream for 10 min before adding iron samples, and kept sealed with a stopper during reaction. The experiments were carried out by putting the flask in a thermostatic shaker bath at 25 ± 0.1 °C, with a rotation speed of 150 rpm. At given time intervals, about 1 mL solution sample were withdrawn and filtered through a 0.22 μm membrane, and Cr(VI) concentration (C_t (mg/L)) in supernatant was measured. The data of batch experiments were obtained in triplicates. The removal of Cr(VI) was calculated according to the equation, removal (%) = $(C_0 - C_t)/C_0 \times 100\%$.

The evaluation on the stability and reusability of iron samples was investigated by repetitive experiments as following: 100 mL solution containing 50 mg/L of Cr(VI) was mixed with NZVI (0.0932 g) or NZVI/Al-bent (0.209 g). After 120 min, 2 mL of solution was withdrawn from the flask for analysis of Cr(VI) concentration, and then an additional 2 mL of concentrated Cr(VI) solution with a proper concentration was added to make sure that the Cr(VI) concentration and pH remained the same at the beginning of four cycles.

2.4. XAFS measurements and analysis

Cr *K*-edge XAFS spectra at 5989 eV for the reference and reacted samples were collected on beamline 14W1 at Shanghai Synchrotron Radiation Facility (SSRF, China). The electron beam energy was 3.5 GeV and the mean stored current was 300 mA. Metallic Cr foil was used to calibrate the energy at 5989 eV. All spectra were collected in fluorescence mode using a multi-element pixel high purity Ge solid-state detector. Scans were collected in triplicate and averaged to improve the signal-to-noise ratio.

Analysis of EXAFS and XANES data was performed using Athena and Artemis interfaces to the IFFEFIT software [31,32]. First, the averaged spectra were normalized with respect to E_0 determined from the second derivative of the raw spectra, and then the total atomic cross-sectional absorption was set to unity. A low-order polynomial function was fit to the pre-edge region and the post-edge region. Next, the data were converted from E-space to k-space and weighted by k^3 to compensate for dampening of the XAFS amplitude with increasing k space. Fourier transformation was then performed over the k range of 2.0–11.0 $Å^{-1}$ using the Kaiser–Bessel window function to obtain the radial structural functions (RSFs). Final fitting of the spectra was done on Fourier transformed k^3-weighted spectra in R-space.

Theoretical EXAFS amplitude and phase functions for Cr–O, Cr–Cr/Fe, and Cr–Al/Si single scattering paths were generated by FEFF 7.0 [33]. Fitted parameters such as interatomic distance (R),

coordination number (N) and Debye–Waller factor (σ^2) were first established with reasonable guesses and were fitted in R-space. The goodness-of-fit parameters were also calculated and compared [34,35]. Errors in individual parameters were ±0.02 Å for R and ±20% for N.

3. Results and discussion

3.1. Macroscopic batch determination

3.1.1. Cr(VI) removal by various zerovalent iron sources

The reductive removal of Cr(VI) by four iron sources (i.e., commercial iron, NZVI, NZVI/Al-bent and NZVI/Na-bent) and the adsorptive removal of Cr(VI) by Al-bent are all shown in Fig. 1. It can be seen that, under identical conditions, the Cr(VI) removal by commercial iron and NZVI after 120 min were 10.6% and 63.0%, respectively. The significantly increased removal of Cr(VI) by NZVI may be related to the much smaller particle size (~100 nm) than commercial iron (~150 μm). The smaller size of iron particles is indicative of larger specific surface area that can offer more reactive sites and higher reactivity [36]. In addition, the removal of Cr(VI) by Al-bent due to adsorption was only 12.4%. More importantly, the Cr(VI) removal by NZVI/Al-bent after 120 min was nearly 100%, which was much higher than that by NZVI, and even distinctly superior to the simple combination of reduction by NZVI and adsorption by Al-bent. This observation indicates that Al-bent as support material in the NZVI treatment system has synergetic effect responsible for the enhanced Cr(VI) removal.

It is well-known that the reduction of Cr(VI) by NZVI is a surface mediated reaction, and thus enrichment of Cr(VI) on solid surface is an important process during Cr(VI) removal [15,37]. The higher Cr(VI) removal by NZVI/Al-bent than that by NZVI/Na-bent (~70% after 120 min) may be attributed to the difference in Cr(VI) adsorption between two bentonites. Fig. 2 shows the adsorption isotherms of Cr(VI) on Na-bent and Al-bent, respectively, indicating the higher adsorption capacity of Al-bent than Na-bent, which could be explained by the electrostatic interaction. It was reported that Na-bent was composed primarily of montmorillonite with negatively charged surface [25], which is unfavorable for adsorption of anionic chromate (CrO_4^{2-} and $HCrO_4^-$) due to electrostatic repulsion. In this work, the Al-bent was obtained from Na-bent by intercalation with poly(hydroxo Al (III)) cations of high positive charge, which could balance the surface charges of Na-bent [25].

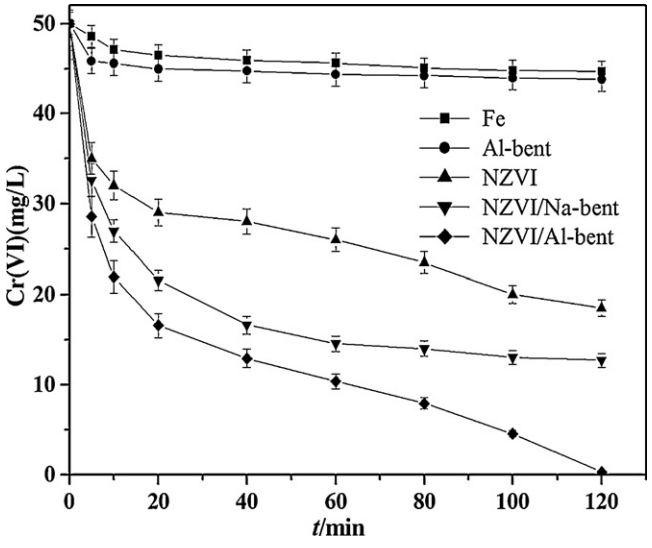

Fig. 1. Removal of Cr(VI) by various iron samples and Al-bent.

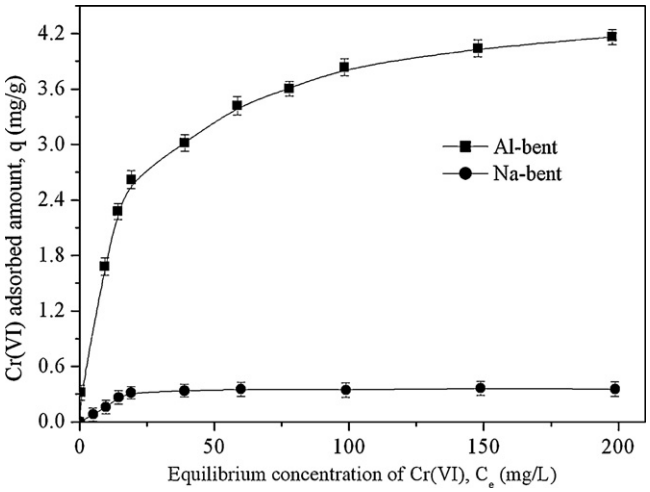

Fig. 2. Adsorption isotherms of Cr(VI) on Na-bent and Al-bent at 25 °C.

Therefore, Al-bent showed higher adsorption for Cr(VI) anions than Na-bent due to the electrostatic interaction. In this way, more Cr(VI) anions can be enriched on the solid phase, making Cr(VI) more easily approach the reactive sites of NZVI supported on Al-bent, and leading to the acceleration of surface reaction. Similar observation has been reported on nitrate removal by NZVI/Al-bent in our previous investigation [26]. These findings highlight the advantages of using pillared bentonites as a support material in the NZVI treatment system.

3.1.2. Effect of initial pH

Fig. 3 shows the effect of pH on Cr(VI) removal by NZVI and NZVI/Al-bent, respectively. The final Cr(VI) removal by NZVI declined from 63.0% to 37.0% when the initial pH increased from 5.0 to 7.0. This indicates that the reduction of Cr(VI) by NZVI is strongly pH-dependent. In ZVI treatment systems, the removal mechanism of Cr(VI) are generally believed to involve adsorption of Cr(VI) on iron surface where electron transfer takes place and then Cr(VI) is reduced to Cr(III) with the oxidation of Fe^0 to Fe^{3+}(see Eq. (1)). Subsequently, a part of Cr(III) precipitates as Cr^{3+} hydroxides and/or mixed Fe^{3+}/Cr^{3+} (oxy)hydroxides (see Eq. (2)) [6,8,37].

$$Cr_2O_7^{2-}(aq) + 2Fe^0(s) + 14H^+(aq) \rightarrow 2Cr^{3+}(aq) + 2Fe^{3+}(aq) + 7H_2O \quad (1)$$

$$xCr^{3+}(aq) + (1-x)Fe^{3+}(aq) + 3H_2O \rightarrow Cr_xFe_{(1-x)}(OH)_3 \downarrow + 3H^+ \quad (2)$$

In general, pH plays an important role during the removal of contaminants by iron [38,39]. It can be clearly see from Eq. (1) that a lower pH favored Cr(VI) reduction, since at lower pH, corrosion of NZVI was accelerated and the precipitation of $Cr(OH)_3$ or $Cr_xFe_{1-x}(OH)_3$ on iron surface was unfavorable, which contributed to the increase of Cr(VI) removal.

However, from Fig. 3B, one can find that the final Cr(VI) removal by NZVI/Al-bent decreased from 100% to 95.1% when the initial pH increased from 5.0 to 7.0, suggesting a less pH influence in this system. This is probably attributed to the buffering effect of aluminol or silanol groups on Al-bent. As pH increased with H^+ being consumed, the aluminol or silanol groups dissociated to compensate the depletion of protons [40]. Powell et al. [39] reported that the presence of aluminosilicate aquifer materials significantly enhanced the Cr(VI) removal by iron. In such a system, protons are generated by dissolution of aluminosilicate minerals along with silica formation, and by subsequent reaction of silica with iron oxides.

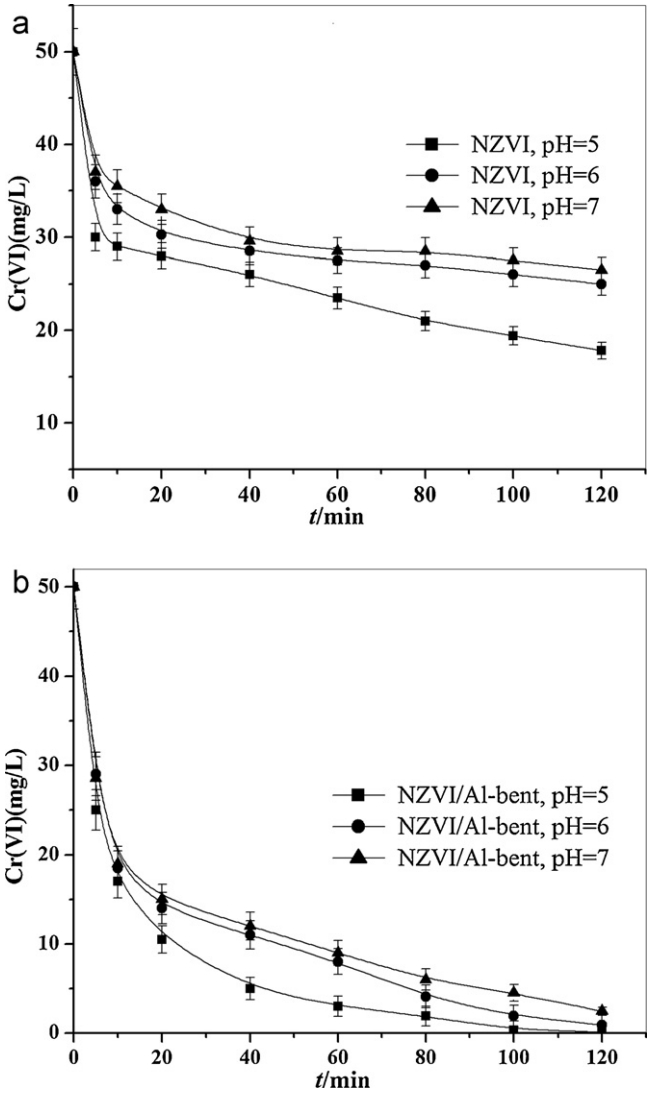

Fig. 3. Removal of Cr(VI) by NZVI (A) or NZVI/Al-bent (B) at various pH values as a function of reaction time.

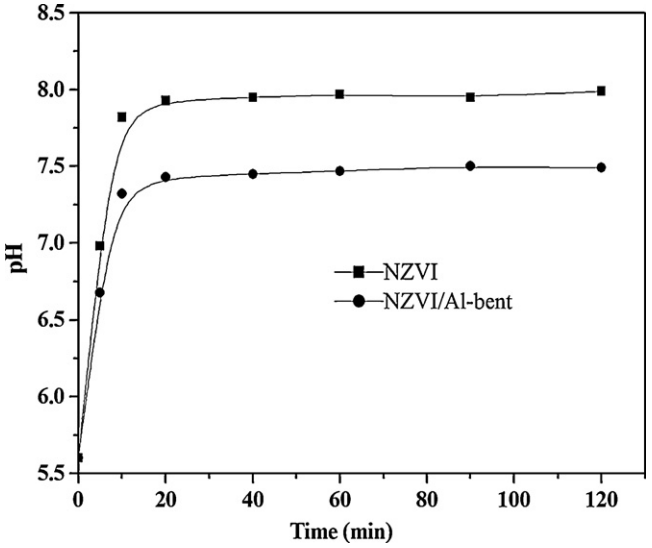

Fig. 4. Variation of pH during the reaction process of Cr(VI) by NZVI and NZVI/Al-bent at initial pH 5.6.

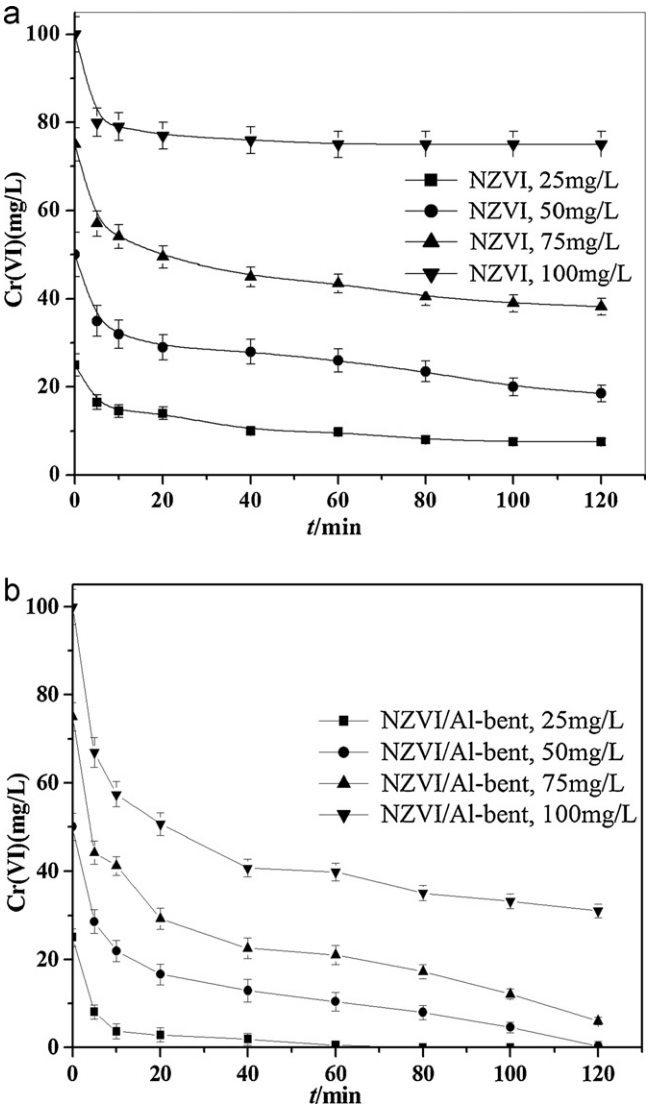

Fig. 5. Removal of Cr(VI) by NZVI (A) or NZVI/Al-bent (B) at various initial Cr(VI) concentrations as a function of reaction time.

The generated protons maintained the low pH and thus reduced the surface passivation of iron. A similar buffering effect has also been reported for quartz in ZVI–Cr(VI) system [41]. The variation of pH during reaction of Cr(VI) by NZVI and NZVI/Al-bent at initial pH 5.6 are shown in Fig. 4, and the results indicate that the introduction of Al-bent as a support material can help maintain the lower pH in the NZVI/Al-bent treatment system (~7.4) than that in the NZVI treatment system (~8.0). This finding is therefore of great significance to remediate Cr(VI) using NZVI/Al-bent over a wide pH range.

3.1.3. Kinetic studies on Cr(VI) removal by NZVI or NZVI/Al-bent

The removal of Cr(VI) by NZVI and NZVI/Al-bent as a function of initial concentration are shown in Fig. 5A and B, respectively. It can be found that the removal by NZVI/Al-bent was always higher than that by NZVI at each initial concentration. Kinetics of NZVI and NZVI/Al-bent reaction is another important aspect concerning their application for environmental remediation. The Langmuir–Hinshelwood (L–H) kinetic model (see Eq. (3)), which has been widely used to describe surface-catalyzed reactions [42],

Table 1
L–H kinetic equation fitting.

Catalysts	Fitted equation	R	k_1 (mg/(L min))	k_2 (L/mg)
NZVI/Al-bent	$\frac{1}{r_0} = 0.106 + 4.82\frac{1}{c_0}$	0.987	9.42	0.0220
NZVI	$\frac{1}{r_0} = 0.130 + 11.4\frac{1}{c_0}$	0.999	7.67	0.0114

was used to investigate Cr(VI) reduction kinetics by NZVI or NZVI/Al-bent.

$$\frac{1}{r_0} = \frac{1}{k_1 k_2} \cdot \frac{1}{c_0} + \frac{1}{k_1} \quad (3)$$

where k_1 and k_2 are reaction rate constant and adsorption coefficient, respectively. They were obtained by fitting the L–H model to the data set of initial reaction rate r_0 at various initial concentrations C_0, and r_0 ($\Delta C/\Delta t$) was calculated from the decreased Cr(VI) concentration ($\Delta C = C_0 - C_t$) in the first 5 min (Δt). The fitting results are shown in Table 1, the correlation coefficients $R > 0.98$ indicate that Cr(VI) reduction by NZVI or NZVI/Al-bent is fitted well to the L–H model. The k_1 and k_2 values for Cr(VI) removal by NZVI/Al-bent were 1.2 and 2.0 times larger than those by bare NZVI, respectively. The results indicate that the reaction rate was positively related to the adsorbed amount of Cr(VI) by iron, and confirm that the removal rate of Cr(VI) by NZVI/Al-bent was accelerated by Al-bent adsorption.

3.1.4. Recycling of NZVI or NZVI/Al-bent

The repeated availability of supported NZVI after many cycles is quite crucial for the practical application. According to the recycling experiments of NZVI and NZVI/Al-bent in Cr(VI) removal, we found that NZVI/Al-bent was valid for at least four cycles as shown in Fig. 6A, with satisfied removal efficiency (95.5%) even in the fourth round. However, the removal by NZVI decreased from 63.0% to 53.1% after four cycles. The results indicate that NZVI/Al-bent displayed much higher stability and reusability than NZVI. Fig. 6B shows the variation of Fe^{3+} concentration in solution during Cr(VI) removal. It can be found that Fe^{3+} released rapidly into solution with Cr(VI) removal by NZVI proceeding. However, in NZVI/Al-bent treatment, much fewer Fe^{3+} ions were detected during the whole reaction. This may be attributed to the adsorption of Fe^{3+} by Al-bent. As Fe^{3+} could cause a secondary pollution in the environment, it is desirable to reduce its release during contaminants removal. The observation indicates that the introduction of Al-bent as a support material in NZVI treatment systems can effectively immobilize Fe^{3+} as the by-product.

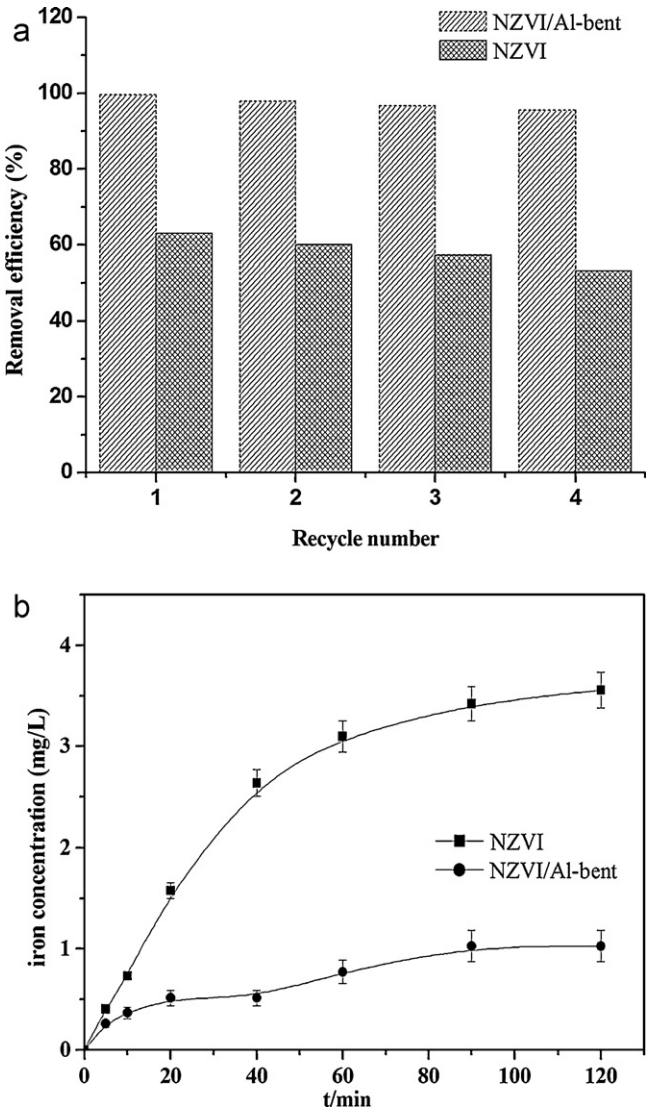

Fig. 6. (A) Recycling for the removal of Cr(VI) by NZVI or NZVI/Al-bent, (B) amount of iron ions released in the solution during the removal of Cr(VI) by NZVI and NZVI/Al-bent.

3.2. Spectroscopic evidence for the enhanced removal of Cr(VI) by NZVI/Al-bent

In order to further provide molecular evidence for the enhanced removal of Cr(VI) by NZVI/Al-bent that resulted from the synergetic effect between Al-bent adsorption and NZVI reduction, but not their simple combination, XAFS spectroscopy was utilized to determine the oxidation state and local coordination structure of Cr(VI) reacted with NZVI and NZVI/Al-bent samples. Cr oxidation state and local coordination structure can be determined by examining the XANES and EXAFS regions of the XAFS spectra [43,44].

Cr *K*-edge XANES and EXAFS spectra were collected from 2.0 mmol/L Cr(VI), Cr(III) reference samples and Cr(VI)-treated Al-bent, NZVI and NZVI/Al-bent samples. Normalized Cr *K*-edge XANES results are shown in Fig. 7. The tetrahedral $Cr(VI)O_4$ compound, which lacks an inversion center, exhibits a pre-edge peak from a dipole-allowed transition of a 1s electron to an unoccupied antibonding t_2^* tetrahedral orbital. In contrast, the absence of this feature is evidence of the octahedral $Cr(III)O_6$ compounds [43,44]. The Cr(VI)-treated Al-bent, without the effects of Cr(VI) reduction, was employed in our study to facilitate analysis of the Cr(VI)-treated NZVI and NZVI/Al-bent samples. As we can see from Fig. 7, Cr XANES spectrum of the Cr(VI)-treated Al-bent sample is quite similar to that of Cr(VI), indicating that the removal of Cr(VI) by Al-bent is an adsorption process. Whereas Cr XANES spectrum of the Cr(VI)-treated NZVI/Al-bent sample is quite similar to that of Cr(III), suggesting that Cr(VI) was completely reduced to Cr(III) under our experimental conditions. Nevertheless, a small pre-edge feature in the Cr XANES spectrum of the Cr(VI)-treated NZVI sample demonstrates that Cr(VI) is partly reduced under identical conditions, therefore, some Cr may be removed by an adsorption mechanism. Aside from the contribution of a trace amount of Cr(VI), the XANES results for the Cr(VI)-treated NZVI sample suggest that the reaction product is mainly Cr(III). In a previous XANES study on Cr(VI)-treated Fe(II)-faujasite sample conducted by Kiser et al. [45], the XANES spectrum for this sample also retained a weak absorption peak at ~5995 eV which is from the Cr(VI) pre-edge feature suggestive of a little amount of unreacted Cr(VI). The results for the Cr(VI)-treated NZVI system are quite similar to those for the Cr(VI)-treated Fe(II)-faujasite system. Surface passivation is an important process in heterogeneous redox reaction and has been observed for the reduction of Cr(VI) by magnetite [44]. In the current study of

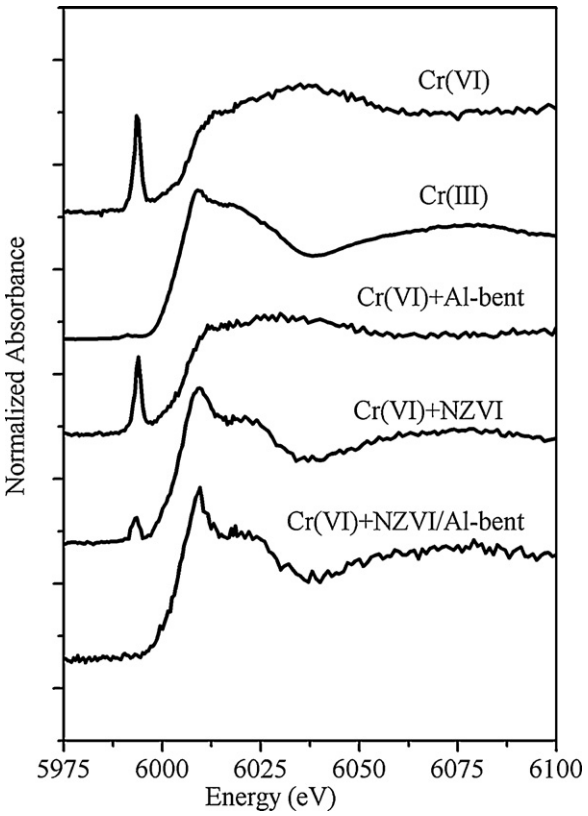

Fig. 7. Cr *K*-edge XANES spectra of reference samples and reacted samples used in this study.

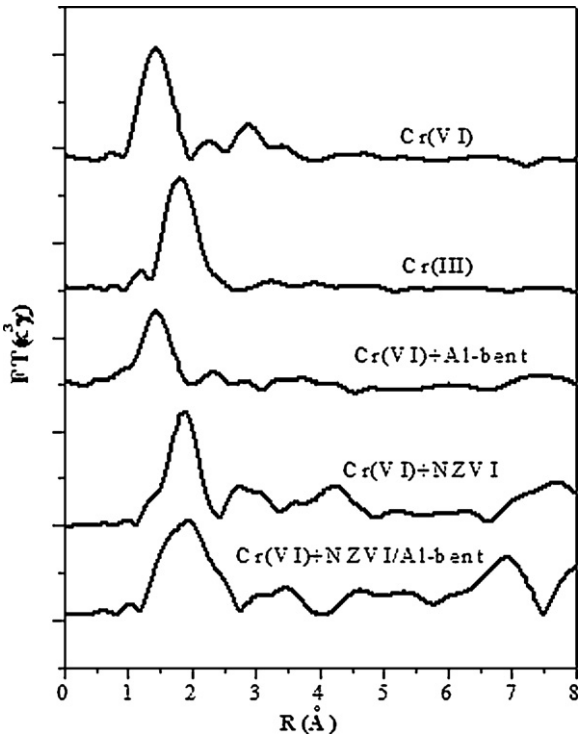

Fig. 8. Fourier transforms of Cr *K*-edge EXAFS spectra of reference samples and reacted samples used in this study.

NZVI-induced reduction of Cr(VI), NZVI can be coated with a thin oxide skin consisting mainly of magnetite. The redox process converted magnetite and NZVI, which are conductive and facilitate electron-transfer processes, to an insulating Fe(III)–Cr(III) oxyhydroxide. The insulating nature of these layers prevented electron transfer from deeper layers, thus bringing the redox process to a halt. Therefore, the residual Cr(VI) in solution can be adsorbed on the resulting iron corrosion products. Lo and co-authors [6,46] have suggested that, although the removal of Cr(VI) by ZVI was mainly through reductive precipitation, a little mount of Cr(VI) might also be removed by adsorption on iron corrosion products. In another report from XPS analysis conducted by Li et al. [47], it was also revealed that Cr(VI) was immobilized on NZVI surface by adsorption and reduction. They suggested the formation of surface Cr^{3+} hydroxides and/or Fe^{3+}/Cr^{3+} (oxy)hydroxides on NZVI gradually increased the resistance for the electron transfer from Fe^0 to Cr(VI), and thus allowed the adsorption of Cr(VI). The current results from XANES investigation are in good agreement with the previous reports [46,47]. These findings, at molecular level, firmly proved that the improved removal of Cr(VI) in the NZVI/Al-bent treatment system is not attributed only to the adsorption of Cr(VI) by Al-bent, but the synergetic effect between Al-bent adsorption and NZVI reduction. It is the adsorption of Al-bent that facilitated the reduction of Cr(VI) by NZVI, leading to the enhancement for the reductive removal of Cr(VI).

EXAFS spectra were employed to determine the local atomic structure of Cr in the Cr(VI)-treated Al-bent, NZVI and NZVI/Al-bent samples. The results of Cr *K*-edge EXAFS spectra are shown in Fig. 8, and the fitted values are given in Table 2. The EXAFS results indicated that after reduction of Cr(VI), Cr(III) became associated with the solid phase. Fitting the 2.0 mmol/L Cr(VI) solution data resulted in a shell of $N = 4$ O atoms with a single Cr–O interatomic distance of $R = 1.66$ Å (Table 2) which is comparable to 1.69 Å reported previously [48]. A small second shell peak was noted but not included in the fit. Fitting the 2.0 mmol/L Cr(III) solution data resulted in a shell of $N = 6$ O atoms with a single Cr–O interatomic distance of $R = 2.01$ Å. The EXAFS data for Cr(VI)-treated Al-bent (Table 2) show a coherent Cr–O shell composed of ~3.7 O atoms at distances of 1.67 Å, which is once again indicative of the adsorption of Cr(VI) on Al-bent. The absence of the second coordination shell in the EXAFS fitting results for this sample indicates that ion exchange or outer-sphere complexation is mainly responsible for the adsorption of Cr(VI) on Al-bent. However, the EXAFS data for Cr(VI)-treated NZVI and NZVI/Al-bent (Table 2) show a coherent Cr–O shell composed of ~6 O atoms at distances of 1.93 and 2.01 Å, respectively. These distances agree well with a Cr–O distance of 1.99 Å found in previous EXAFS work on synthetic $Cr(OH)_3 \cdot nH_2O$ precipitate [49], Cr(III) adsorption complexes on hydrous Fe(III) oxides [50], and Cr(III) surface precipitates on silica [48]. What's more, the fit of the second shell corresponds to a Cr–Cr/Fe bond at 3.05 Å with $N \sim 3$. Since the photoelectron backscattering function of Fe and Cr are similar, it is not possible to use EXAFS spectra to distinguish between these two possible second-shell atoms [44,51]. The Cr–Fe distances of Cr(VI)-treated NZVI and NZVI/Al-bent

Table 2
EXAFS results of reference samples and reacted samples at Cr *K*-edge.

Reacted sample	Shell	*R* (Å)	*N*	σ^2 (Å^2)
Cr(VI)	Cr–O	1.66	4.0	0.004
Cr(III)	Cr–O	2.01	6.0	0.005
Cr(VI) + Al-bent	Cr–O	1.67	3.7	0.004
Cr(VI) + NZVI	Cr–O	1.93	5.3	0.006
	Cr–Fe/Cr	3.06	2.9	0.007
Cr(VI) + NZVI/Al-bent	Cr–O	2.01	5.8	0.004
	Cr–Fe/Cr	3.05	2.7	0.007
	Cr–Al/Si	3.43	1.3	0.007

R – interatomic distance; *N* – number of neighbor atoms; σ^2 – Debye–Waller factor, Cr(VI) and Cr(III) are named as reference samples, whereas the others as reacted samples.

samples are quite different from that of Cr(VI)-treated α-FeOOH sample, of which the Cr–Fe distance is 337 Å with $N \sim 1.5$ [45]. This is due to the fact that Cr(VI) anion directly adsorption to α-FeOOH surface by inner-sphere complexation and remains on α-FeOOH surface in the form of Cr(VI), whereas Cr(VI) was reduced by NZVI and NZVI/Al-bent and mainly remains in the form of Cr(III) on NZVI and NZVI/Al-bent surface, respectively. The Cr–O distance determined in the current system is similar to that of the co-precipitates formed in the homogeneous system, wherein Cr(VI) was reduced by aqueous Fe(II) [51]; however, the Cr–Cr/Fe distance is slightly larger than that was determined for the coprecipitates in the homogeneous system [51]. This may be due to the fact that in the heterogeneous system, reduction of Cr(VI) causes precipitation of $Fe_{1-x}Cr_x(OH)_3$ or $Cr(OH)_3$ deposited on NZVI surface. But in the homogeneous system, where Cr(VI) is reduced by Fe^{2+} or ferrous hydrolysis species, reduced Cr and oxidized Fe forms co-precipitates [44,51]. This observation shows that Cr(VI) reduced by NZVI and NZVI/Al-bent have essentially similar microscopic structural environments. More importantly, the fits for Cr(VI)-treated NZVI/Al-bent sample also yields a Cr–Al/Si bond at 3.43 Å with $N \sim 1$, which is absent in the Cr(VI)-treated NZVI sample. This distance agrees well with a Cr–Si distance of 3.51 Å found in a previous report [45]. The photoelectron backscattering function of Al and Si are similar, and thus it is not possible to use EXAFS spectra to distinguish between these two possible second-shell atoms. Based on the EXAFS results it can be reasonably assumed that that some insoluble Cr(III) species produced during reduction of Cr(VI) by NZVI/Al-bent might be transferred to the surface of Al-bent, therefore the insoluble products of Cr(III) hydroxides or Cr(III)/Fe(III) hydroxides on iron surface could be greatly reduced. It is an important reason for the enhanced reactivity and stability of NZVI by introduction of Al-bent as a support material.

4. Conclusions

Though legitimate concerns have been raised about the suitability of NZVI for environmental applications due to particle aggregation and stability, technological advances such as particle surface modification will overcome these problems. In this study, the enhanced reactivity and reusability of NZVI were obtained by dispersing it on an adsorptive support (Al-bent), and the mechanism for the enhancement was revealed by XAFS investigations. Our results suggest that the pillared bentonite, as an important support material, can play multiple roles in the supported NZVI system, including the enrichment of contaminants, pH buffering and transferring precipitates from iron surface. This study also demonstrated the utility of XAFS to elucidate the mechanism for removal of contaminants by supported NZVI. The information presented herein is important for scientists and engineers to develop better models to use supported NZVI for environmental remediation.

Acknowledgements

This work was supported by the National Natural Science Foundation of China (20977063, 21177088). The authors acknowledge Dr. Guodong Sheng (Institute of Plasma Physics, Chinese Academy of Science) for the XAFS determination and analysis. The authors also gratefully acknowledge Prof. Yuying Huang and Dr. Xing Gao (SSRF, China) for helpful technical assistance on XAFS experiments.

References

[1] J. Dries, L. Bastiaens, D. Springael, S.N. Agathos, L. Diels, Competition for sorption and degradation of chlorinated ethenes in batch zero-valent iron systems, Environ. Sci. Technol. 38 (2004) 2879–2884.
[2] J. Dries, L. Bastiaens, D. Springael, S.N. Agathos, L. Diels, Combined removal of chlorinated ethenes and heavy metals by zerovalent iron in batch and continuous flow column systems, Environ. Sci. Technol. 39 (2005) 8460–8465.
[3] J. Klausen, J. Ranke, R. Schwarzenbach, Influence of solution composition and column aging on the reduction of nitroaromatic compounds by zero-valent iron, Chemosphere 44 (2001) 511–517.
[4] J.N. Fiedor, W.D. Bostick, R.J. Jarabek, J. Farrell, Understanding the mechanism of uranium removal from groundwater by zero-valent iron using x-ray photoelectron spectroscopy, Environ. Sci. Technol. 32 (1998) 1466–1473.
[5] S.J. Morrison, D.R. Metzler, C.E. Carpenter, Uranium precipitation in a permeable reactive barrier by progressive irreversible dissolution of zero-valent iron, Environ. Sci. Technol. 35 (2001) 385–390.
[6] T. Liu, P. Rao, M.S.H. Mak, P. Wang, I.M.C. Lo, Removal of co-present chromate and arsenate by zero-valent iron in groundwater with humic acid and bicarbonate, Water Res. 43 (2009) 2540–2548.
[7] M.S.H. Mak, P. Rao, I.M.C. Lo, Effects of hardness and alkalinity on the removal of arsenic(V) from humic acid-deficient and humic acid-rich groundwater by zero-valent iron, Water Res. 43 (2009) 4296–4304.
[8] I.M.C. Lo, C.S.C. Lam, K.C.K. Lai, Hardness and carbonate effects on the reactivity of zero-valent iron for Cr(VI) removal, Water Res. 40 (2006) 595–605.
[9] S.M. Ponder, J.G. Darab, T.E. Mallouk, Remediation of Cr(VI) and Pb(II) aqueous solutions using supported, nanoscale zero-valent iron, Environ. Sci. Technol. 34 (2000) 2564–2569.
[10] S.M. Ponder, J.G. Darab, J. Bucher, D. Caulder, I. Craig, L. Davis, N. Edelstein, W. Lukens, H. Nitsche, L. Rao, D.K. Shuh, T.E. Mallouk, Surface chemistry and electrochemistry of supported zerovalent iron nanoparticles in the remediation of aqueous metal contaminants, Chem. Mater. 13 (2001) 479–486.
[11] H. Song, E.R. Carraway, Reduction of chlorinated ethanes by nanosized zero-valent iron: kinetics, pathways, and effects of reaction conditions, Environ. Sci. Technol. 39 (2005) 6237–6245.
[12] T. Phenrat, N. Saleh, K. Sirk, R.D. Tilton, G.V. Lowry, Aggregation and sedimentation of aqueous nanoscale zerovalent iron dispersions, Environ. Sci. Technol. 41 (2006) 284–290.
[13] Y. Liu, G.V. Lowry, Effect of particle age (Fe^0 content) and solution pH on NZVI reactivity: H^2 evolution and TCE dechlorination, Environ. Sci. Technol. 40 (2006) 6085–6090.
[14] Y. Liu, T. Phenrat, G.V. Lowry, Effect of TCE concentration and dissolved groundwater solutes on NZVI-promoted TCE dechlorination and H_2 evolution, Environ. Sci. Technol. 41 (2007) 7881–7887.
[15] L.B. Hoch, E.J. Mack, B.W. Hydutsky, J.M. Hershman, J.M. Skluzacek, T.E. Mallouk, Carbothermal synthesis of carbon-supported nanoscale zero-valent iron particles for the remediation of hexavalent chromium, Environ. Sci. Technol. 42 (2008) 2600–2605.
[16] J. Zhan, I. Kolesnichenko, B. Sunkara, J. He, G.L. McPherson, G. Piringer, V.T. John, Multifunctional iron–carbon nanocomposites through an aerosol-based process for the in situ remediation of chlorinated hydrocarbons, Environ. Sci. Technol. 45 (2011) 1949–1954.
[17] B. Sunkara, J. Zhan, I. Kolesnichenko, Y. Wang, J. He, J.E. Holland, G.L. McPherson, V.T. John, Modifying metal nanoparticle placement on carbon supports using an aerosol-based process, with application to the environmental remediation of chlorinated hydrocarbons, Langmuir 27 (2011) 7854–7859.
[18] F. He, D.Y. Zhao, Preparation and characterization of a new class of starch-stabilized bimetallic nanoparticles for degradation of chlorinated hydrocarbons in water, Environ. Sci. Technol. 39 (2005) 3314–3320.
[19] N. Sakulchaicharoen, D. O'Carroll, J. Herrera, Enhanced stability and dechlorination activity of pre-synthesis stabilized nanoscale FePd particles, J. Contam. Hydrol. 118 (2010) 117–127.
[20] T. Zheng, J. Zhan, J. He, C. Day, Y. Lu, G.L. McPerson, G. Piringer, V.T. John, Reactivity characteristics of nanoscale zerovalent iron-silica composites for trichloroethylene remediation, Environ. Sci. Technol. 42 (2008) 4494–4499.
[21] J. Zhan, T. Zheng, G. Piringer, C. Day, G.L. McPerson, Y. Lu, K. Papadopoulos, V.T. John, Transport characteristics of nanoscale functional zerovalent iron/silica composites for in situ remediation of trichloroethylene, Environ. Sci. Technol. 42 (2008) 8871–8876.
[22] J. Li, Y. Li, Q. Meng, Removal of nitrate by zero valent iron and pillared bentonite, J. Hazard. Mater. 174 (2010) 188–193.
[23] L.N. Shi, Y.M. Lin, X. Zhang, Z. Chen, Synthesis, characterization and kinetics of bentonite supported nZVI for the removal of Cr(VI) from aqueous solution, Chem. Eng. J. 171 (2011) 612–617.
[24] L.Z. Zhu, X.X. Ruan, B.L. Chen, R.L. Zhu, Efficient removal and mechanisms of water soluble aromatic contaminants by a reduced-charge bentonite modified with benzyltrimethylammonium cation, Chemosphere 70 (2008) 1987–1994.
[25] S. Zhao, C.H. Feng, X.N. Huang, B.H. Li, J.F. Niu, Z.Y. Shen, Role of uniform pore structure and high positive charges in the arsenate adsorption performance of Al_{13}-modified montmorillonite, J. Hazard. Mater. 203-204 (2012) 317–325.
[26] Y. Zhang, Y. Li, H. Dong, J. Li, X. Zheng, Enhanced removal of nitrate by a novel composite: Nanoscale zero valent iron supported on pillared clay, Chem. Eng. J. 171 (2011) 526–531.
[27] Y. Zhang, Y. Li, X. Zheng, Removal of atrazine by nanoscale zero valent iron supported on organobentonite, Sci. Total Environ. 409 (2011) 625–630.
[28] Y. Li, Y. Zhang, J. Li, X. Zheng, Enhanced removal of pentachlorophenol by a novel composite: nanoscale zero valent iron immobilized on organobentonite, Environ. Pollut. 159 (2011) 3744–3749.
[29] A. Vazquez, M. López, G. Kortaberria, L. Martín, I. Mondragon, Modification of montmorillonite with cationic surfactants. Thermal and chemical analysis including CEC determination, Appl. Clay Sci. 41 (2008) 24–36.

[30] G. Den Boef, A. Hulanicki, D.T. Burns, Spectrophotometric and fluo-rimetric methods, in: T.S. West, H.W. The Late, Nurnberg (Eds.), The Determination of Trace Metals in Natural Waters, Blackwell Scientific Publications, Oxford, 1988.
[31] S.M. Webb, SIXPACK: a graphical user interface for XAS analysis using IFEFFIT, Phys. Scripta T 115 (2005) 1011–1014.
[32] M. Newville, IFEFFIT: interactive XAFS analysis and FEFF fitting, J. Synchrotron Rad. 8 (2001) 324–332.
[33] J.J. Rehr, S.I. Zabinsky, R.C. Albers, High-order multiple scattering calculations of X-ray absorption fine structure, Phys. Rev. Lett. 69 (1992) 3397–3400.
[34] S.E. Fendorf, M.J. Eick, P. Grossl, D.L. Sparks, Arsenate and chromate retention mechanisms on goethite. 1. Surface structure, Environ. Sci. Technol. 31 (1997) 315–320.
[35] M. Schlegel, A. Manceau, D. Chateigner, L. Charlet, Sorption of metal ions on clay minerals. I. Polarized EXAFS evidence for the adsorption of Co on the edges of hectorite particles, J. Colloid Interf. Sci. 215 (1999) 140–158.
[36] R. Cheng, J. Wang, W. Zhang, Comparison of reductive dechlorination of p-chlorophenol using Fe^0 and nanosized Fe^0, J. Hazard. Mater. 144 (2007) 334–339.
[37] T. Liu, D.C.W. Tsang, I.M.C. Lo, Chromium(VI) reduction kinetics by zero-valent iron in moderately hard water with humic acid: iron dissolution and humic acid adsorption, Environ. Sci. Technol. 42 (2008) 2092–2098.
[38] R.M. Powell, R.W. Puls, S.K. Hightower, D.A. Sabatini, Coupled iron corrosion and chromate reduction: mechanisms for subsurface remediation, Environ. Sci. Technol. 29 (1995) 1913–1922.
[39] R.M. Powell, R.W. Puls, Proton generation by dissolution of intrinsic or augmented aluminosilicate minerals for in situ contaminant remediation by zero-valence-state iron, Environ. Sci. Technol. 31 (1997) 2244–2251.
[40] Y.J. Oh, H. Song, W.S. Shin, S.J. Choi, Y.H. Kim, Effect of amorphous silica and silica sand on removal of chromium(ε) by zero-valent iron, Chemosphere 66 (2007) 858–865.
[41] D.W. Blowes, C.J. Ptacek, J.L. Jambor, In situ remediation of Cr(VI)-contaminated groundwater using permeable reactive walls: laboratory studies, Environ. Sci. Technol. 31 (1997) 3348–3357.
[42] V. Janda, P. Vasek, J. Bizova, Z. Belohlav, Kinetic models for volatile chlorinated hydrocarbons removal by zero valent iron, Chemosphere 54 (2004) 917–925.
[43] M.L. Peterson, A.F. White, G.E. Brown, G.A. Parks, Surface passivation of magnetite by reaction with aqueous Cr(VI): XAFS and TEM results, Environ. Sci. Technol. 31 (1997) 1573–1576.
[44] Y.T. He, S.J. Traina, Cr(VI) reduction and immobilization by magnetite under alkaline pH conditions: the role of passivation, Environ. Sci. Technol. 39 (2005) 4499–4504.
[45] J.R. Kiser, B.A. Manning, Reduction and immobilization of chromium(VI) by iron(II)-treated Faujasite, J. Hazard. Mater. 174 (2010) 167–174.
[46] M.S.H. Mak, P. Rao, I.M.C. Lo, Zero-valent iron and iron oxide-coated sand as a combination for removal of co-present chromate and arsenate from groundwater with humic acid, Environ. Pollut. 159 (2011) 377–382.
[47] X. Li, J. Cao, W. Zhang, Stoichiometry of Cr(VI) immobilization using nanoscale zero-valent iron (nZVI): a study with high-resolution X-ray photoelectron spectroscopy (HR-XPS), Ind. Eng. Chem. Res. 47 (2008) 2131–2139.
[48] S.E. Fendorf, G.M. Lamble, M.G. Stapleton, M.J. Kelley, D.L. Sparks, Mechanisms of chromium(III) sorption on silica. 1. Cr(III) surface structure derived by extended X-ray absorption fine structure spectroscopy, Environ. Sci. Technol. 28 (1994) 204–289.
[49] A.A. Manceau, L. Charlet, X-ray absorption spectroscopic study of the sorption of Cr(III) at the oxide–water interface. I. Molecular mechanism of Cr(III) oxidation on Mn oxides, J. Colloid Interf. Sci. 148 (1992) 425–442.
[50] L. Charlet, A.A. Manceau, X-ray absorption spectroscopic study of the sorption of Cr(III) at the oxide–water interface. II. Adsorption, coprecipitation, and surface precipitation on hydrous ferric oxide, J. Colloid Interf. Sci. 148 (1992) 443–458.
[51] Y.T. He, C.C. Chen, S.J. Traina, Inhibited Cr(VI) reduction by aqueous Fe(II) under hyper-alkaline conditions, Environ. Sci. Technol. 38 (2004) 5535–5539.